Chaotic dynamics of the Kepler problem with oscillating singularity

Alessandro Margheri*

Fac. Ciências da Univ. de Lisboa e CMAF-CIO,
Campo Grande, Edifício C6, piso 2, P-1749-016 Lisboa Portugal
e-mail: amargheri@fc.ul.pt

and

Pedro J. Torres†

Departamento de Matemática Aplicada,
Facultad de Ciencias, Universidad de Granada, 18071 Granada, Spain
e-mail: ptorres@ugr.es

Abstract

We prove the presence of chaotic dynamics for the classical two-body Kepler problem with a time-periodic gravitational coefficient oscillating between two fixed values. The set of chaotic solutions we detect is coded by the number of revolutions in each period. The chaotic dynamics is obtained for large period T as well as for small angular momentum μ. In particular, we provide an explicit lower bound on T and explicit upper bound on μ which guarantee the existence of complex dynamics. We get our results by applying a simple and well known topological method, the *stretching along the path* technique. Our results are robust with respect to small perturbations of the gravitational coefficient and to the addition of a small friction term.

Keywords: Gyldén problem, solar radiation pressure, periodic solution, chaos, stretching along paths

*Supported by Fundação para a Ciência e Tecnologia, UID/MAT/04561/2013 and project PTDC/MAT/113383/2009

†Supported by project MTM2014-52232-P, Ministerio de Economía y Competitividad, Spain

1 Introduction

The motivation of this paper is to study some aspects of the dynamics of the system

$$\ddot{u} = -h(t)\frac{u}{|u|^3}, \tag{1.1}$$

where $h(t)$ is a T-periodic function. This model can be regarded as a Kepler problem with a fluctuating gravitational parameter, and with this interpretation $h(t)$ should be positive for every t. Nevertheless, negative values for $h(t)$ are justified if we take into account the photogravitational effect, that is, the effect of solar radiation pressure. Imagine a body (a small asteroid or spacecraft) of mass m that is orbiting around a star of luminosity $L(t)$ of mass $M >> m$. The cross-section to mass ratio of the body is called the *sailing capacity*, denoted by $\sigma(t)$. In a spacecraft or artificial satellite, this parameter can be modulated by manoeuvring a solar sail. If the sailing capacity is significant, there is an interplay between the attractive gravitational force and the repulsive force due to the solar radiation pressure exerted by the star, in such a way that the motion of the body is ruled by system (1.1) with

$$h(t) = GM - \frac{\sigma(t)L(t)}{4\pi c},$$

where G is the gravitational constant and c the speed of light in the vacuum (see for instance [14]). Eventually, the effect of the solar radiation pressure may be stronger than the gravitational force, leading to negative values of $h(t)$.

Originally, system (1.1) was proposed by Gyldén to explain the secular acceleration observed in the Moon's longitude, but nowadays it is mainly used to study the photogrativational effect described above, that may strongly affect the global dynamics of the model. For different mathematical approaches to this problem, one can consult the papers [2, 6, 4, 13, 14, 15, 16, 17] and the references therein.

Our model is an example of central force field. Every solution $u(t)$ of (1.1) lies in a plane through the origin and perpendicular to the angular momentum $u(t) \wedge \dot{u}(t) = u(0) \wedge \dot{u}(0)$, which is a conserved quantity. In what follows we consider orbits with the same angular momentum $u(0) \wedge \dot{u}(0) \neq 0$, so that they all belong to the same plane, which from now on we identify with $\mathbb{R}^2$. Introducing in it polar coordinates

$$u(t) = x(t)\big(\cos\theta(t), \sin\theta(t)\big)$$

with polar radius $x(t) = |u(t)| > 0$ and angle $\theta(t) \in \mathbb{R}$ for every t, system (1.1) is equivalent to

$$\ddot{x} = \frac{\mu^2}{x^3} - \frac{h(t)}{x^2}, \tag{1.2}$$

and $\dot{\theta} = \frac{\mu}{x^2}$, where $\mu = |u(0) \wedge \dot{u}(0)|$. Notice that equation (1.1) is invariant under the group of rotations with center in the origin. As a consequence, a solution $x(t)$ of (1.2) determines uniquely, modulo the initial angle θ_0, a solution of (1.1).

Our objective is to provide sufficient conditions such that (1.2), and hence (1.1) has chaotic dynamics, with periodic orbits of any period, when the restriction of $h(t)$ to the interval $[0, T]$ is a piecewise constant function of the form

$$h(t) = \begin{cases} h_1 & \text{if } t \in [0, T_1] \\ h_2 & \text{if } t \in]T_1, T_1 + T_2 =: T]. \end{cases} \tag{1.3}$$

This particular choice of $h(t)$, which, of course, does not allow to tackle the general model, may seem just of mathematical interest. However, it can actually represent meaningful physical systems. For instance, one can think about an artificial satellite orbiting around a star with fixed luminosity and with a cross-section changing periodically in a piecewise constant way by means of a solar sail. In addition, our results are robust under suitable small perturbations, as we will see later. This means, in particular, that $h(t)$ may actually be a smooth function which is a small deformation of the stepwise one defined by (1.3).

In dynamical terms, the chaotic solutions we find are characterized by the number of revolutions made in each period T. Such number will vary in an apparently random way, following any prescribed bounded sequence of positive integers, where the bound depends on the period. These solutions are obtained considering two different types of conditions. In the first type it is assumed that the period T is above an explicitly given threshold. Generally speaking, this case corresponds to a large period T. The second kind of conditions take advantage of the fact that, fixed T_1 and T_2, one can make the threshold mentioned above tend to zero as μ tends to zero. This singles out an explicit upper bound on μ, below which chaotic solutions exist.

Our proofs are based on a simple topological method to detect periodic points and chaotic orbits that is applied to the Poincaré map associated to a first order planar system equivalent to (1.2). The method, called the "stretching along the path" (SAP for short), was developed, essentially, in [10](but see also, for example, [7, 11] for a recent presentation of this approach with different applications). Its application to ODEs requires, in general, a simple but careful phase plane analysis, which often allows to enter the setting of the theory of the generalized linked twist maps (LTMs) (see [8] and references therein). A generalized LTM ϕ is the composition of two continuous maps, $\phi = \phi_2 \circ \phi_1$ each acting on a topological annulus as a twist map. The annuli (one of which may be of 'infinite radius', i.e. a topological strip, in which case ϕ is called 'bend-twist' map) are linked through regions homeomorphic to the unit square. If the twist on the boundaries of the annuli is sufficiently strong, the SAP method guarantees the existence of complex dynamics for ϕ, with periodic points of any period, in the topological rectangles which realize the link. This is the general framework which we will use to obtain our results.

It is worth to mention that the possibility to apply the SAP method to the Gyldén model in order to detect chaotic dynamics was suggested in the recent monograph [19] (see Section 4.6 therein).

In the next section we will state explicitly the definition of chaos we consider and recall briefly the SAP technique as well as the general theorem we will use

to detect chaos. The phase plane analysis necessary for the application of the SAP method is performed in Section 3. The main mathematical results for equation (1.1) are contained in Section 4 and Section 5. Section 4 is focused on the case when the function $h(t)$ takes values of different sign, whereas Section 5 analyzes the case of a positive $h(t)$. Finally, in Section 6 we show that, as a consequence of our main results, chaotic dynamics is found in sets of solutions with small angular momentum.

2 Definition of chaos and SAP method

The complex dynamics for a map ϕ may be defined in terms of the erratic and unpredictable form in which many of its orbits $\{x_n = \phi^n(x) : n \geq 0\}$, move between suitable subsets, say $\mathcal{K}_0, \cdots \mathcal{K}_p$, of its domain. This behaviour is described by encoding the orbits with sequences of symbols $(s_0, s_1, \ldots, s_n \ldots)$, where $s_k \in \{1, \cdots, p\}$ means that $\phi^k(x) \in K_{s_k}$. Chaos will occur for ϕ when we are able to reproduce with its orbits a sufficiently broad set of sequence of symbols.

Since we will work in the phase plane, all definitions will be given in $\mathbb{R}^2$ (rather than in a general metric space.)

We start with our precise definition of chaotic dynamics.

Definition 1. *Let $\phi : D_\phi (\subseteq \mathbb{R}^2) \to \mathbb{R}^2$ a map and let $\mathcal{D} \subseteq D_\phi$ be a nonempty set. We say that ϕ induces chaotic dynamics on $p \geq 2$ symbols in the set $\mathcal{D}$ if there exist p nonempty pairwise disjoint compact sets*

$$\mathcal{K}_1, \cdots, \mathcal{K}_p \subseteq \mathcal{D}$$

such that, for each two–sided sequence of p symbols

$$(s_i)_{i\in\mathbb{Z}} \in \Sigma_p := \{1, \cdots, p\}^{\mathbb{Z}},$$

there exists a corresponding sequence $(w_i)_{i\in\mathbb{Z}} \in \mathcal{D}^{\mathbb{Z}}$ with

$$w_i \in \mathcal{K}_{s_i} \quad \text{and} \quad w_{i+1} = \phi(w_i), \ \ \forall\, i \in \mathbb{Z} \tag{2.1}$$

and, whenever $(s_i)_{i\in\mathbb{Z}}$ is a $k-$periodic sequence (that is, $s_{i+k} = s_i\,, \forall i \in \mathbb{Z}$) for some $k \geq 1$, there exists a $k-$periodic sequence $(w_i)_{i\in\mathbb{Z}} \in \mathcal{D}^{\mathbb{Z}}$ satisfying (2.1).

A consequence of the previous definition is that, when ϕ is continuous and injective, as is the case for a Poincaré map, there exists a compact set $\Lambda \subset \bigcup_{i=1}^{p} \mathcal{K}_i$ which is ϕ invariant (that is $\phi(\Lambda) = \Lambda$) and such that $\phi_{|\Lambda}$ is semiconjugated with the Bernoulli shift on two symbols. We recall that the Bernoulli shift on p symbols $\sigma : \Sigma_p \to \Sigma_p$ is defined by $\sigma : (s_i)_i \mapsto (s_{i+1})_i$ and represents the model of chaotic map, since it displays various important features (like transitivity, sensitive dependence on the initial points, density of periodic orbits,

positive topological entropy) associated to complex dynamics. The semiconjugation between ϕ and σ means that there exists a continuous and onto function $g : \Lambda \to \Sigma_p$ such that $\sigma \circ g = g \circ \phi$. Loosely speaking, the existence of the semiconjugation g implies that the chaotic dynamics of σ on Σ_p provides a lower bound for the complexity of the dynamics of $\phi_{|\Lambda}$. Hence, even without the reference to the periodic points, the existence of g is considered by some authors as a possible definition of chaotic dynamics (see, for example [1, 3]). However, as a consequence of Definition 1 we can take an invariant set Λ containing as a dense subset the periodic points of ϕ and such that the counterimage (by the semiconjugacy g) of any periodic sequence $(s_i)_i$ in Σ_p contains a periodic point of ϕ having the same period of $(s_i)_i$ (see [7] for the details).

We recall now the key technique that we use to detect chaotic dynamics on p symbols according to Definition 1, the "stretching along the path"(SAP) method. The sets on which it applies are oriented topological rectangles, denoted by $\widehat{\mathcal{R}} := (\mathcal{R}, \mathcal{R}^-)$, where $\mathcal{R}$ is a subset of $\mathbb{R}^2$ homeomorphic the unit square $[0,1]^2$ (a "curvilinear rectangle" in our applications) oriented by choosing two compact disjoint arcs in its boundary (two "opposite sides") $\mathcal{R}^- = \mathcal{R}_l^- \cup \mathcal{R}_r^-$. The letters r and l stand for "left" and "right" and their use is merely conventional. In the same spirit, we will also use the letters u and d ("up" and "down") for the chosen opposite sides.

The SAP property provides a notion of topological crossing between a topological oriented rectangle and its image through a map ϕ which allows to obtain the existence of a fixed point for ϕ. Its precise definition is presented below the in a slightly simplified form.

Suppose that $\phi : D_\phi (\subseteq \mathbb{R}^2) \to \mathbb{R}^2$ is a continuous map defined on a set D_ϕ. Let $\widehat{\mathcal{P}} := (\mathcal{P}, \mathcal{P}^-)$ and $\widehat{\mathcal{Q}} := (\mathcal{Q}, \mathcal{Q}^-)$ be oriented rectangles in D_ϕ.

Definition 2. *Let $\mathcal{H} \subseteq \mathcal{P}$ be a compact set. We say that $(\mathcal{H}, \phi)$ stretches $\widehat{\mathcal{P}}$ to $\widehat{\mathcal{Q}}$ along the paths and write*

$$(\mathcal{H}, \phi) : \widehat{\mathcal{P}} \twoheadrightarrow \widehat{\mathcal{Q}},$$

if the following condition hold:

- *for every path $\gamma : [t_0, t_1] \to \mathcal{P}$ such that $\gamma(t_0) \in \mathcal{P}_l^-$ and $\gamma(t_1) \in \mathcal{P}_r^-$ (or $\gamma(t_0) \in \mathcal{P}_r^-$ and $\gamma(t_1) \in \mathcal{P}_l^-$), there exists a subinterval $[t', t''] \subseteq [t_0, t_1]$ such that*

$$\gamma(t) \in \mathcal{H}, \quad \phi(\gamma(t)) \in \mathcal{Q}\,, \ \ \forall\, t \in [t', t'']$$

and, moreover, $\phi(\gamma(t'))$ and $\phi(\gamma(t''))$ belong to different components of $\mathcal{Q}^-$.

Broadly speaking, $(\mathcal{H}, \phi) : \widehat{\mathcal{P}} \twoheadrightarrow \widehat{\mathcal{Q}}$ means that there is a subset $\mathcal{H}$ of $\mathcal{P}$ such that any path in $\mathcal{P}$ connecting the two opposite sides of $\mathcal{P}^-$ has a subpath which is contained in $\mathcal{H}$ and is stretched by ϕ across $\mathcal{Q}$ from $\mathcal{Q}_l^-$ to $\mathcal{Q}_r^-$ (see Figure 2.1). As proved in [12], when $(\mathcal{H}_i, \phi) : \widehat{\mathcal{P}} \twoheadrightarrow \widehat{\mathcal{P}}$ for at least $p \geq 2$

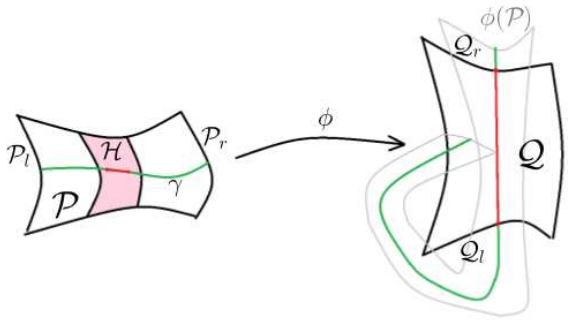

Figure 2.1: A graphical illustration of the SAP property

nonempty pairwise disjoint sets $\mathcal{H}_1, \dots, \mathcal{H}_p$, then we have complex dynamics on p symbols for ϕ according to Definition 1 (see also [11, Theorems 2.2-2.3]). In fact, the existence of such $\mathcal{H}_i$ correspond to p "topologically correct" crossings between $\mathcal{P}$ and $\phi(\mathcal{P})$ which allow to code the orbits of ϕ with arbitrary sequences of p symbols and to get the existence of periodic points of ϕ, obtained as fixed points of suitable iterates of ϕ.

We point out that other approaches to complex dynamics either do not guarantee the existence of the periodic points of ϕ ([5]) or rely on the computation of suitable sophisticated homological invariants such as, for example, the Conley index ([9]) or the Lefschetz fixed point index ([18]). In comparison, the SAP technique provides a simpler but effective tool to detect chaotic dynamics and the existence of periodic solutions of any period in some ODEs models.

In the application considered in this paper the Poincaré operator ϕ will naturally factor as the composition of two maps. In this situation, our results will be consequence of the following theorem, which corresponds to Theorem 2.1 in [8] and to Theorem 3.2 in [11].

Theorem 1. *Let $\phi_1 : D_{\phi_1}(\subseteq \mathbb{R}^2) \to \mathbb{R}^2$ and $\phi_2 : D_{\phi_2}(\subseteq \mathbb{R}^2) \to \mathbb{R}^2$ be continuous maps and let $\widehat{\mathcal{P}} := (\mathcal{P}, \mathcal{P}^-)$ and $\widehat{\mathcal{Q}} := (\mathcal{Q}, \mathcal{Q}^-)$ be oriented rectangles in D_{ϕ_1} and D_{ϕ_2}, respectively. Suppose that the following conditions are satisfied:*

(H_{ϕ_1}) *there exist $m \geq 1$ pairwise disjoint compact sets $\mathcal{H}_1, \dots, \mathcal{H}_m \subseteq \mathcal{P}$ such that $(\mathcal{H}_i, \phi_1) : \widehat{\mathcal{P}} \twoheadrightarrow \widehat{\mathcal{Q}}$, for $i = 1, \dots, m$;*

(H_{ϕ_2}) *there exist $\ell \geq 1$ pairwise disjoint compact sets $\mathcal{K}_1, \dots, \mathcal{K}_\ell \subseteq \mathcal{Q}$ such that $(\mathcal{K}_i, \phi_2) : \widehat{\mathcal{Q}} \twoheadrightarrow \widehat{\mathcal{P}}$, for $i = 1, \dots, \ell$.*

If at least one between m and ℓ is greater or equal than 2, then the map $\phi := \phi_2 \circ \phi_1$ induces chaotic dynamics on $m \times \ell$ symbols in the set

$$\mathcal{H}^* := \bigcup_{\substack{i=1,\dots,m \\ j=1,\dots,\ell}} \mathcal{H}'_{i,j} \quad \text{with } \mathcal{H}'_{i,j} := \mathcal{H}_i \cap \phi_1^{-1}(\mathcal{K}_j).$$

In the framework of the previous result the orbits $(w_n)_{n\in\mathbb{Z}}$ of $\phi = \phi_2 \circ \phi_1$ are coded by sequences of pairs of positive integers $\mathbf{s} = (s_n)_n = (p_n, q_n)_n \in \{1, \dots, m\}^{\mathbb{Z}} \times \{1, \dots, \ell\}^{\mathbb{Z}}$ according to the rule $w_n \in \mathcal{H}'_{p_n,q_n}$. This rule means that $w_n \in \mathcal{H}_{p_n}$ and $w_{n+1} = \phi_1(w_n) \in \mathcal{K}_{q_n}$.

If either $m = 1$ or $l = 1$ we go back, essentially, to the setting of Definition 1. In fact, if for example $l = 1$, as it will be in our first main result, Theorem 2 below, the sequences which encode the trajectories are of the form $(s_n)_n = (p_n, 1)_n$. The symbol 1 in the second component encodes some dynamical information, but it is qualitatively the same for all orbits, and therefore it does not contribute to their erratic behaviour, which is determined only by $(p_n)_n$. Therefore, in this case we will still write that ϕ induces chaotic dynamics on m symbols rather than on $m \times 1$ symbols.

3 Analysis of phase portraits

To prepare the setting for the application of the SAP method to our problem, in this section we carry out the analysis of the phase planes associated to equation (1.2) when $h(t)$ is piecewise constant and takes two values in each period.

If $h(t)$ satisfies (1.3), equation (1.2) takes the form

$$\ddot{x} = \begin{cases} \frac{\mu^2}{x^3} - \frac{h_1}{x^2} & \text{if } t \in [iT, iT + T_1] \\ \frac{\mu^2}{x^3} - \frac{h_2}{x^2} & \text{if } t \in]iT + T_1, iT + T_1 + T_2 := (i+1)T], \end{cases} \tag{3.1}$$

with $i \in \mathbb{Z}$. The solutions of equations (3.1) are a chain of segments of solutions of two periodically alternating autonomous equations of the form

$$\ddot{x} = \frac{\mu^2}{x^3} - \frac{h}{x^2}. \tag{3.2}$$

Since we will consider that h_2 can be either positive or negative, in this section we analyse the phase portrait of the planar system, equivalent to (3.2),

$$\begin{cases} \dot{x} = y, \\ \dot{y} = \frac{\mu^2}{x^3} - \frac{h}{x^2}. \end{cases}$$

when $h > 0$ and when $h < 0$.

By defining the potential energy

$$F_h(x) = -\frac{\mu^2}{2x^2} + \frac{h}{x},$$

the trajectories of (1.2) are the level curves of the energy function

$$V_h(x, y) = \frac{y^2}{2} - F_h(x).$$

All the orbits of this system are defined for $t \in \mathbb{R}$.

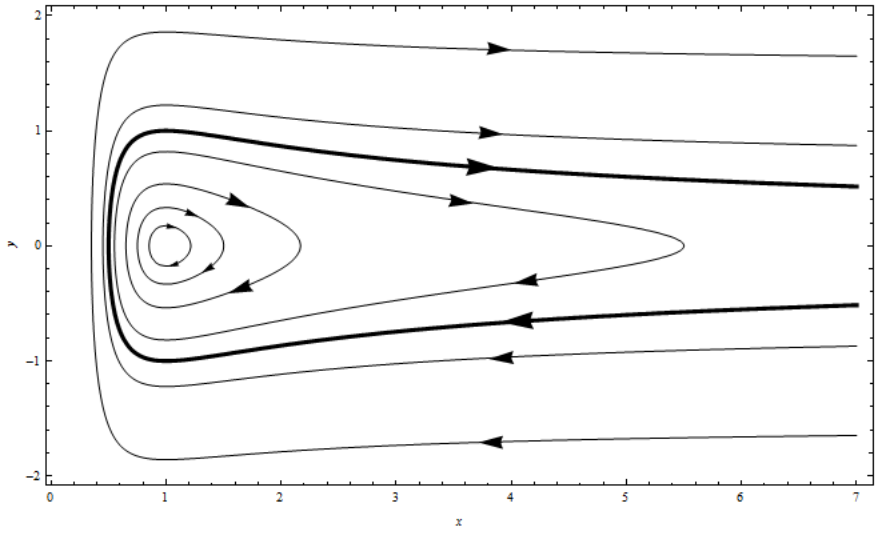

Figure 3.1: Phase plane of eq. (3.2) with $h > 0$. The thick curve corresponds to the parabolic orbit.

First, we analyze the case $h > 0$. With a slight abuse of the terminology, we will call parabolic, elliptic, hyperbolic orbits the solutions of (1.2) which describe the evolution of the radial component of, respectively, parabolic, elliptic, hyperbolic orbits of the corresponding Kepler problem. There exists a parabolic orbit with implicit equation

$$V_h(x, y) = 0,$$

which separates hyperbolic orbits from elliptic ones (see Fig. 3.1). Elliptic orbits rotate around the unique equilibrium $(\frac{\mu^2}{h}, 0)$ (which corresponds to a circular orbit of the Kepler problem) and can be written as

$$V_h(x, y) = -F_h(d),$$

with $\frac{\mu^2}{2h} < d < \frac{\mu^2}{h}$. In this way, the elliptic cycles are parametrized according to d. The minimum x value (pericenter) and the maximum x value (apocenter) of the corresponding orbit are given respectively by

$$x_{min}(d) = d, \quad x_{max}(d) = \frac{h}{F_h(d)} - d. \tag{3.3}$$

Moreover, by Kepler's third law, the period of the corresponding orbit is given by

$$T_h(d) = \frac{\pi h}{\sqrt{2}}[F_h(d)]^{-\frac{3}{2}}. \tag{3.4}$$

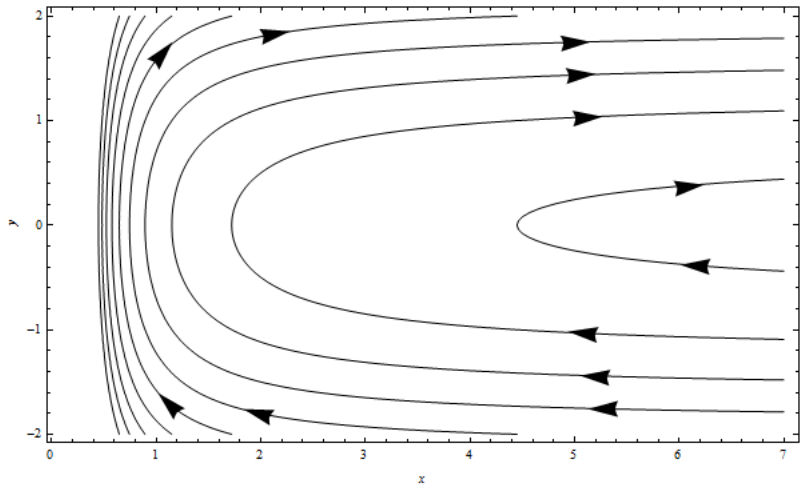

Figure 3.2: Phase plane of eq. (3.2) with $h < 0$.

On the other hand, when $h < 0$ the phase curves are given by

$$V_h(x, y) = C$$

for $C > 0$ (see Fig. 3.2). For a given $C > 0$, the corresponding orbit is defined for every

$$x \geq x_C = \frac{-h + \sqrt{h^2 + 2\mu^2 C}}{2C}.$$

Note that x_C is a decreasing function of of C and that $x_C \to +\infty$ as $C \to 0^+$.

In order to enter the setting suitable for stating and proving our results, we rewrite equation (3.1) in the equivalent form

$$\begin{cases} \dot{x} = y \\ \dot{y} = \frac{\mu^2}{x^3} - \frac{h(t)}{x^2} \end{cases} \tag{3.5}$$

where $t \in \mathbb{R}$ and $h(t)$ is defined by (1.3). The Poincaré map of system (3.5) is well defined as a homeomorphism of the half-plane $\mathbb{R}^+ \times \mathbb{R} = \{(x, y) : x > 0\}$ onto itself by

$$\phi : \mathbb{R}^+ \times \mathbb{R} \to \mathbb{R}^+ \times \mathbb{R} \quad \phi(z_0) = (x(T, z_0), y(T, z_0)),$$

where $(x(\cdot, z_0), y(\cdot, z_0))$ is the solution of system (3.5) with initial condition $(x(0), y(0)) = z_0 = (x_0, y_0)$. The map ϕ can be decomposed as

$$\phi = \phi_1 \circ \phi_2 \,,$$

where, $\phi_i(z),\ i=1,2,$ is the point at time T_i of the solution of the autonomous system

$$(Eq_i)\begin{cases} \dot{x}=y \\ \dot{y}=\frac{\mu^2}{x^3}-\frac{h_i}{x^2} \end{cases}$$

starting from $z\in\mathbb{R}^2$ at time $t=0$.

In what follows, we will tackle the complex behaviour of solutions of (3.1) considering the two cases $h_1>0, h_2<0$ and $h_1>0, h_2>0$.

4 The case $h_1>0$, $h_2<0$.

In this section we consider the case when $h_1>0$, $h_2<0$. In the solar sail model referred in the introduction, it corresponds to a situation where the solar radiation pressure exceeds the gravitational attraction force during some interval of time. Our main result is as follow.

Theorem 2. *For any choice of the positive integer $m\geq 2$ and of the time $T_2>0$, there exists T_1^* such that if $T_1>T_1^*$, equation (3.1) exhibits chaotic dynamics on m symbols.*

In terms of the dynamical properties of the solutions of (1.1) our result reads as follows. Let $s:=(s_i)_{i\in\mathbb{Z}}$ be an arbitrary two-sided sequence of integers, with $0\leq s_i\leq m-1$ for each $i\in\mathbb{Z}$. Then, there exists a solution $\tilde{u}(\cdot)$ of equation (1.2) which satisfies the following properties:

-when $t\in[iT, iT+T_1]$, $\tilde{u}(t)$ describes an elliptic orbit (which depends on i) passing s_i+1 times from the apocenter and s_i times from the pericenter;

-when $t\in]iT+T_1,(i+1)T[$ the function $x(t)=|\tilde{u}(t)|$ is strictly convex and has exactly one minimum.

Moreover, if the sequence s_i is k-periodic (for some $k\geq 1$), namely, $s_{i+k}=s_i$ for all $i\in\mathbb{Z}$, then there exists at least one solution $\tilde{u}(\cdot)$ with the properties described above and such that $\tilde{u}(t+kT)=\tilde{u}(t)$, for each $t\in\mathbb{R}$.

The result is stable with respect to small perturbations. In particular, for any fixed $T_1>T_1^*$ there is $\varepsilon>0$ such that for each measurable T-periodic weight $q(t)$ satisfying

$$\int_0^T |q(t)-h(t)|\leq\varepsilon$$

and each constant $c\in\mathbb{R}$ with

$$|c|\leq\varepsilon,$$

the perturbed equation

$$u''+cu'=-q(t)\frac{u}{|u|^3}$$

has solutions with the same behaviour as the one described above.

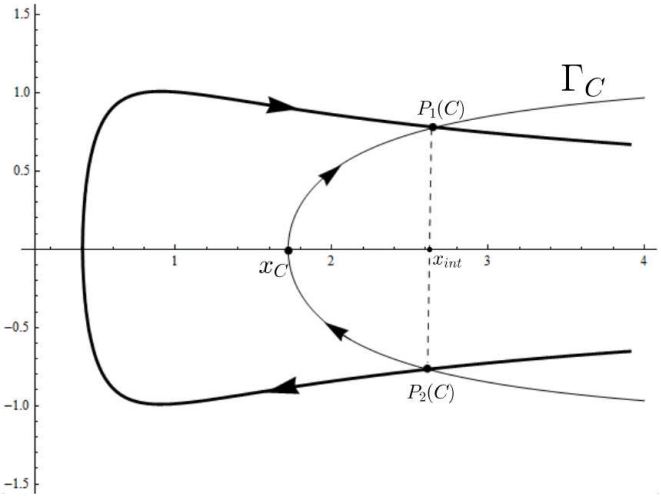

Figure 4.1: Intersection of the parabolic orbit with Γ_C.

Note that the function $q(t)$ above may be chosen in the class of smooth functions.

The chaotic dynamics will be obtained in a topological rectangle $\mathcal{P}$ of the phase plane which links a topological annulus and a topological strip on which the Poincaré operator ϕ acts as a bend-twist map.

The rest of the section is devoted to the proof of Theorem 2.

4.1 Linking of phase portraits.

The parabolic orbit of the autonomous system (Eq_1) is given by

$$V_{h_1}(x, y) = 0. \tag{4.1}$$

We are interested in the intersection of such curve with the orbits of the autonomous system (Eq_2), which are given by

$$\Gamma_C = \{(x, y) \,:\, V_{h_2}(x, y) = C\}\,, \qquad C > 0. \tag{4.2}$$

It is not difficult to check that curves (4.1)-(4.2) has exactly two different points of intersection, $P_1(C)$ and $P_2(C)$, with abscissa

$$x_{int} = \frac{h_1 - h_2}{C}$$

if and only if $0 < C < \frac{2h_1}{\mu^2}(h_1 - h_2)$ (see Fig. 4.1). The time of travel between the points $(x_C, 0)$ and $P_1(C)$ along the trajectory Γ_C can be explicitly computed

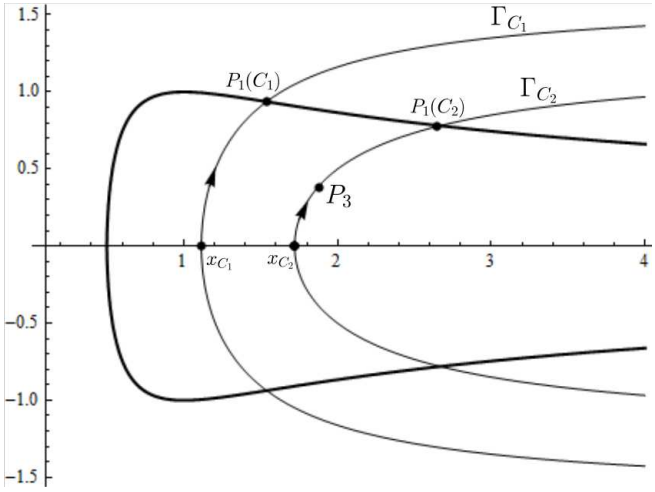

Figure 4.2: Intersection of the parabolic orbit with the orbits $\Gamma_{C_1}, \Gamma_{C_2}$ and the position of the point P_3.

as

$$\tau(C) = \int_{x_C}^{x_{int}} \frac{u}{\sqrt{2Cu^2 + 2h_2u - \mu^2}} du = \\ = \frac{1}{2C^{3/2}} \left[\sqrt{2h_1^2 - 2h_1h_2 - \mu^2 C} + \frac{h_2}{\sqrt{2}} \log \left(\frac{\sqrt{h_2^2 + 2\mu^2 C}}{2h_1 - h_2 + \sqrt{4h_1^2 - 4h_1h_2 - 2\mu^2 C}} \right) \right].$$

Elementary but lengthy computations prove that $\tau(C)$ is a strictly decreasing function of C such that

$$\lim_{C \to 0^+} \tau(C) = +\infty, \qquad \lim_{C \to \frac{2h_1}{\mu^2}(h_1 - h_2)} \tau(C) = 0. \tag{4.3}$$

4.2 Construction of the oriented topological rectangles.

In this subsection, we are going to construct the oriented topological rectangles needed to prove the existence of chaotic dynamics by means of the SAP method. This is done through several steps:

Step 1. By using (4.3), there exists a unique $0 < C_1 < \frac{2h_1}{\mu^2}(h_1 - h_2)$ such that $T_2 = \tau(C_1)$.

Step 2. Choose $C_2 < C_1$. For the corresponding orbits $\Gamma_{C_1}, \Gamma_{C_2}$, one has $\tau(C_1) < \tau(C_2)$.

Step 3. Let us define the point $P_3 := \phi_2(x_{C_2}, 0)$ (see Figure 4.2). Of course, P_3

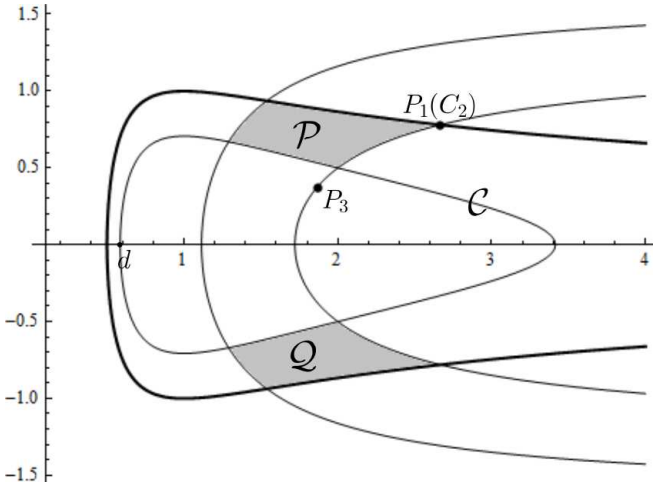

Figure 4.3: Construction of the topological rectangles $\mathcal{P}, \mathcal{Q}$.

belongs to the orbit γ_{C_2}. More explicitly, x_3 is determined by solving the equation

$$\int_{x_{C_2}}^{x_3} \frac{u}{\sqrt{2C_2u^2 + 2h_2u - \mu^2}} du = T_2,$$

and then letting

$$y_3 = \sqrt{2C_2 + \frac{2h_2}{x_3} - \frac{\mu^2}{x_3^2}}.$$

Since $\tau(C_1) < \tau(C_2)$, P_3 is located on the segment of the orbit Γ_{C_2} determined by $(x_{C_2}, 0)$ and $P_1(C_2)$.

Step 4. Select a cycle

$$\mathcal{C} = \{(x, y) \,:\, V_{h_1}(x, y) = -F_{h_1}(d)\}, \quad \frac{\mu^2}{2h_1} < d < \frac{\mu^2}{h_1},$$

of the autonomous system (Eq_1) choosing d close enough to $\frac{\mu^2}{2h_1}$, as to guarantee that $\mathcal{C}$ crosses the x axis to the left of x_{C_1}, has only two intersections with Γ_{C_1} and intersects the segment of orbit Γ_{C_2} determined by P_3 and $P_1(C_2)$ (see Fig. 4.3).

Now, we are ready to construct the topological rectangles as follows:

$$\mathcal{P} = \{(x, y) \,:\, y > 0, -F_{h_1}(d) \le V_{h_1}(x, y) \le 0, C_2 \le V_{h_2}(x, y) \le C_1\},$$

$$\mathcal{Q} = \{(x, -y) \,:\, (x, y) \in \mathcal{P}\}.$$

Figure 4.3 provides a graphical illustration. The suitable orientation on $\mathcal{P}$ is

obtained by choosing its "up" and "down" sides. More formally $\widehat{\mathcal{P}} = (\mathcal{P}, \mathcal{P}^-)$ where $\mathcal{P}^- = \partial\mathcal{P}_u \cup \partial\mathcal{P}_d$ and

$$\partial\mathcal{P}_u = \{(x,y) \in \mathcal{P} \,:\, V_{h_1}(x,y) = 0\},$$
$$\partial\mathcal{P}_d = \{(x,y) \in \mathcal{P} \,:\, V_{h_1}(x,y) = -F_{h_1}(d)\}.$$

The proper orientation on $\mathcal{Q}$ is obtained selecting its "left" and "right" sides, namely $\widehat{\mathcal{Q}} = (\mathcal{Q}, \mathcal{Q}^-)$ where $\mathcal{Q}^- = \partial\mathcal{Q}_l \cup \partial\mathcal{Q}_r$ and

$$\partial\mathcal{Q}_l = \{(x,y) \in \mathcal{Q} \,:\, V_{h_2}(x,y) = C_1\},$$
$$\partial\mathcal{Q}_r = \{(x,y) \in \mathcal{Q} \,:\, V_{h_2}(x,y) = C_2\}$$

4.3 Proof of Theorem 2.

Define

$$T_1^* = mT(\mathcal{C}) \tag{4.4}$$

where

$$T(\mathcal{C}) = \frac{\pi h_1}{\sqrt{2}}[F_{h_1}(d)]^{-3/2}.$$

is the period of the cycle $\mathcal{C}$ of the autonomous system (Eq_1) and take $T_1 > T_1^*$.

Fix a curve γ in $\mathcal{P}$ joining $\partial\mathcal{P}_d$ and $\partial\mathcal{P}_u$. Following the evolution of γ under the flow given by system (Eq_1) on the time interval $[0, T_1]$, at time T_1 we get a curve, $\phi_1(\gamma)$, which winds around the the equilibrium $(\frac{\mu^2}{h_1}, 0)$ at least $m-1$ times and whose intersection with $\mathcal{Q}$ contains m arcs joining $\partial\mathcal{Q}_r$ and $\partial\mathcal{Q}_l$ (see Fig. 4.4 for a graphical illustration of this crossing property when $m = 2$). These curves correspond to subarcs of γ made of initial conditions $z = (x, y)$ of solutions $(x(t), y(t))$ of (Eq_1) which at time T_1 crossed the x axis $1, 3, \cdots, 2m-1$ times. As a consequence, if we denote by $\mathbf{n}(z)$ the number of zeros of the y component of of the solution of (Eq_1) associated to the initial condition z, then the sets

$$\mathcal{H}_i = \{z \in \mathcal{P} : \ \phi_1(z) \in \mathcal{P} \text{ and } \mathbf{n}(z) = 2i+1\}, \ \ i = 0, \cdots m-1,$$

are non empty disjoint compact subsets of $\mathcal{P}$. Moreover, $(\mathcal{H}_i, \phi_1) : \widehat{\mathcal{P}} \overset{\curvearrowright}{\Rightarrow} \widehat{\mathcal{Q}}$, for $i = 0, \ldots, m-1$ and assumption (H_{ϕ_1}) of Theorem 1 is satisfied.

Let now consider a curve γ in $\mathcal{Q}$ joining $\partial\mathcal{Q}_r$ and $\partial\mathcal{Q}_l$. Its image at time $T = T_1 + T_2$ under the flow of system (Eq_2) on the time interval $[T_1, T]$ gives a curve, $\phi_2(\gamma)$, that crosses $\mathcal{P}$ and containing a subarc in $\mathcal{P}$ which joins $\partial\mathcal{P}_d$ and $\partial\mathcal{P}_u$ (see Figure 4.5).

As a consequence, the set

$$\mathcal{K}_1 = \mathcal{Q} \cap \phi_2^{-1}(\mathcal{P})$$

is a nonempty compact subset of $\mathcal{Q}$ and $(\mathcal{K}_1, \phi_2) : \widehat{\mathcal{Q}} \overset{\curvearrowright}{\Rightarrow} \widehat{\mathcal{P}}$. Then, also assumption (H_{ϕ_2}) of Theorem 1 is satisfied with $l = 1$, and we conclude that $\phi = \phi_2 \circ \phi_1$

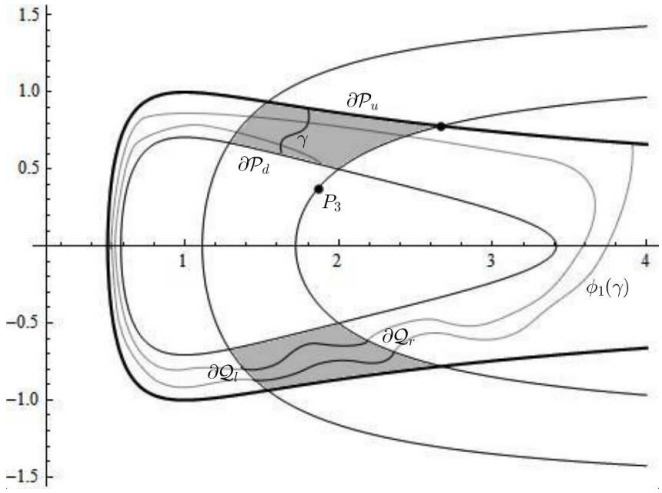

Figure 4.4: An illustration of the SAP property for ϕ_1 when $m = 2$. The image under ϕ_1 of any curve γ in $\mathcal{P}$ joining $\partial\mathcal{P}_d$ and $\partial\mathcal{P}_u$ is a curve which winds around the equilibrium of (Eq_1) and whose intersection with $\mathcal{Q}$ contains two curves joining $\partial\mathcal{Q}_r$ and $\partial\mathcal{Q}_l$.

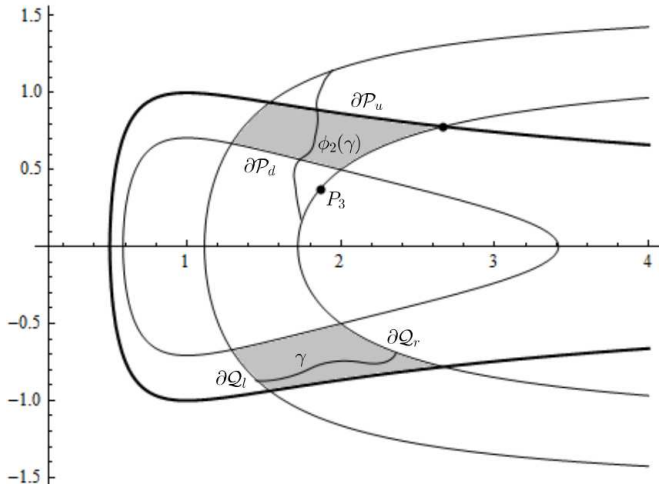

Figure 4.5: The image under ϕ_2 of any curve in $\mathcal{Q}$ joining $\partial\mathcal{Q}_r$ and $\partial\mathcal{Q}_l$ is a curve that crosses $\mathcal{P}$ vertically.

induces chaotic dynamics on $m = m \times 1$ symbols in

$$\bigcup_{i=0}^{m-1} \mathcal{H}^*_{i,1} \subset \mathcal{P},$$

where $\mathcal{H}^*_{i,1} = \mathcal{H}_i \cap \phi_1^{-1}(\mathcal{K}_1)$

The dynamical description of the chaotic solutions follows recalling that a solution $x(t)$ of (1.2) define uniquely, modulo a rotation, a solution $u(t)$ of (1.1) with $h(t)$ defined by (1.3). Then, the zeros of the y component of the phase curve $(x(t), y(t))$ in $[iT, iT + T_1[$ correspond to passages through the apocenter and pericenter along the elliptic orbit (which depends on i) defined by $u_{|[iT,iT+T_1[}$, where $u(t)$ is the solution of the Kepler problem with $h = h_1$. Moreover, the first component $x(t)$ of a solution of (Eq_2) is convex in the interval $[T_1, T]$ and has a strict minimum in $]T_1, T[$. This completes our description.

The stability of the above result under small perturbations is a standard fact which follows, essentially, arguing like in [8][Theorem 4.2] and we omit its proof. □

5 The case $h_1 > 0$, $h_2 > 0$.

When $h_1 > 0$, $h_2 > 0$, equation (1.2) oscillates between two Kepler equations

$$\ddot{x} = \frac{\mu^2}{x^3} - \frac{h_1}{x^2}, \quad t \in [iT, iT + T_1[, \tag{5.1}$$

and

$$\ddot{x} = \frac{\mu^2}{x^3} - \frac{h_2}{x^2}, \ t \in [iT + T_1 + T_2 = (i+1)T[, \tag{5.2}$$

where $i \in \mathbb{Z}$. In this case, considering the corresponding equivalent first order systems (Eq_1) and (Eq_2), the complex dynamics may be obtained entering the setting of the generalized linked twist maps. In this framework, we note that it is possible to carry out two different constructions of the linking among the trajectories of these systems which allow to optimize the lower bound on the period $T = T_1 + T_2$ for which chaotic dynamics occurs (see Remark 1 below). Broadly speaking, the chaotic dynamics will be described by the erratic number of revolutions made in each period by many solutions of (Eq_1) and (Eq_2).

We will sketch just the proof of the first result. The second one may be easily obtained from the ideas presented before and the corresponding phase portrait (see Fig. 5.2).

We recall that systems (Eq_k), $k = 1, 2$ have closed trajectories of the form

$$\frac{y^2}{2} = F_k(x) - F_k(d), \qquad k = 1, 2,$$

where

$$F_k(x) = \frac{h_k}{x} - \frac{\mu^2}{2x^2}, \qquad k = 1, 2, \tag{5.3}$$

and $\frac{h_k}{2\mu^2} < d < \frac{h_k}{\mu^2}$. The value $d = \frac{h_k}{2\mu^2}$ corresponds to the parabolic orbit. Moreover, by (3.4), the period of the closed orbits of (5.1) and of (5.2) through $(d, 0)$ is given, respectively for $k = 1$ and $k = 2$, by

$$T_k(d) = \frac{\pi h_k}{\sqrt{2}} F_k(d)^{-3/2} = \frac{\pi h_k}{\sqrt{2}} F_k(x_k(d))^{-3/2},$$

where by definition

$$x_k(d) = \frac{h_k}{F_k(d)} - d.$$

The function $F_k(d)$ is decreasing on $\left]\frac{h_k}{2\mu^2}, \frac{h_k}{\mu^2}\right[$, and the limits

$$\lim_{d \to \frac{h_k}{2\mu^2}} T_k(d) = +\infty, \quad \lim_{d \to \frac{h_k}{\mu^2}} T_k(d) = \frac{\pi h_k}{\sqrt{2}} F_k\left(\frac{h_k}{\mu^2}\right)^{-3/2}$$

hold for $k = 1, 2$.

Now, we are prepared to state the main results of this section. From now on, without loss of generality, we assume that $h_1 > h_2$. We distinguish two cases. In the first one, the equilibrium of system (Eq_1) is "inside" the parabolic orbit of system (Eq_2), whereas in the second case such equilibrium is "outside".

Theorem 3. *Let us suppose that $h_1 < 2h_2$. Let m and l be two positive integers one of which greater or equal than 2. For a fixed $d \in \left]\frac{\mu^2}{h_1}, \frac{\mu^2}{h_2}\right[$, let us assume that*

$a_1)$ $T_1 > T_1^* = (m+2)\dfrac{T_1(x_2(d))\, T_1(d)}{T_1(x_2(d)) - T_1(d)}$

$a_2)$ $T_2 > T_2^* = (l+2)\dfrac{T_2\left(\frac{\mu^2}{h_1}\right) T_2(d)}{T_2\left(\frac{\mu^2}{h_1}\right) - T_2(d)}$

Then, system (3.1) exhibits chaotic dynamics on $m \times l$ symbols.

In terms of the dynamical properties of the solutions of (1.1) our result reads as follows. Let $k_1 = \lfloor \frac{T_1}{T_1(x_2(d))} \rfloor$ and $k_2 = \lfloor \frac{T_2}{T_2(\mu^2/h_1)} \rfloor$. Let $s := (s_i)_{i\in\mathbb{Z}} = (p_i, q_i)_{i\in\mathbb{Z}}$ be an arbitrary two-sided sequence with $0 \le p_i \le m-1$ and $0 \le q_i \le l-1$ for each $i \in \mathbb{Z}$. Then, there exists a solution $\tilde{u}(\cdot)$ of equation (1.2) with the following properties.

-when $t \in [iT, iT + T_1]$, $\tilde{u}(t)$ describes an elliptic orbit (which depends on i) passing $k_1 + p_i + 2$ times from the apocenter and $k_1 + p_i + 1$ times from the pericenter;

- when $t \in]iT + T_1, (i+1)T[$, $\tilde{u}(t)$ describes an elliptic orbit (which depends on i) passing $k_2 + q_i + 1$ times from the apocenter and $k_2 + q_i + 2$ times from the pericenter.

Moreover, if the sequence s_i is k-periodic (for some $k \ge 1$), namely, $s_{i+k} = s_i$ for all $i \in \mathbb{Z}$, then there exists at least one solution $\tilde{u}(\cdot)$ with the properties described above and such that $\tilde{u}(t + kT) = \tilde{u}(t)$, for each $t \in \mathbb{R}$. This result is stable with respect to the small perturbations considered in Theorem 2

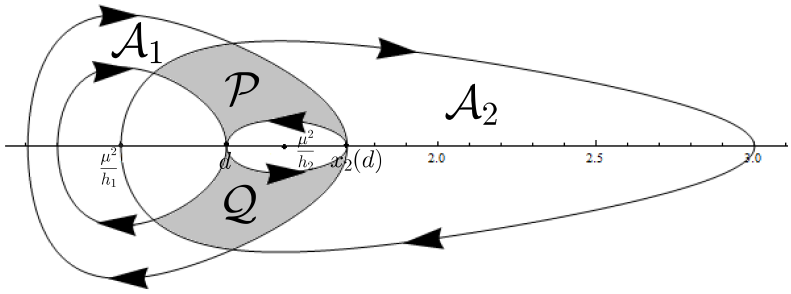

Figure 5.1: Geometry of linking considered in Theorem 3

Proof. The proof is similar to the one of Theorem 2, and therefore we will just outline it, pointing out the main differences. Fixed $d \in \left]\frac{\mu^2}{h_1}, \frac{\mu^2}{h_2}\right[$, we construct a first annulus $\mathcal{A}_1$ with inner boundary given by the cycle of (5.1) passing through $(d, 0)$, and outer boundary given by the cycle of (5.1) passing through $(x_2(d), 0)$. A second annulus $\mathcal{A}_2$ is constructed by taking the cycles of (5.2) passing through $(d, 0)$ and $(\frac{\mu^2}{h_1}, 0)$ as inner and outer boundaries respectively (see Figure 5.1) By construction, such annuli are linked and the intersection is composed by two topological rectangles, $\mathcal{P}$ in the upper half plane and $\mathcal{Q}$ in lower half plane. The orientation considered on these rectangles is the same than the one considered in Theorem 2. Namely, $\mathcal{P}$ is oriented choosing the "up" and "down" sides and $\mathcal{Q}$ is oriented choosing its "left" and "right" sides. Consider now polar coordinates with center in $(\frac{\mu^2}{h_1}, 0)$ with angular coordinate θ increasing in the clockwise sense and such that $\theta \in [0, \pi]$ for the points in $\mathcal{P}$.

The twist condition a_1) guarantees that the gap between the angular coordinates of the image through ϕ_1 of the endpoints of any curve γ in $\mathcal{P}$ joining its "up" and 'down" sides is greater than $2m\pi$ (see e.g. [8][proof of Theorem 4.1 with $L^1_{int} = L^1_{out} = 1/2$]). As a consequence, $\phi_1(\gamma)$ contains m distinct sub arcs included in $\mathcal{Q}$ and joining its "left" and "right" sides. Actually, the angular coordinate of the image of the endpoint of γ on the "up" side, on the slower cycle, lies in $[2\pi k_1, 2\pi k_1 + 2\pi[$ whereas the angular coordinate of image of the endpoint of γ on the "down" side, on the faster cycle, is greater or equal than $2\pi k_1 + 2(m+1)\pi$. Hence, if we denote by $\mathbf{n_1}(z)$ the number of zeros of the y component of the solution of (Eq_1) associated to the initial condition z, then the sets

$$\mathcal{H}_i = \{z \in \mathcal{P} : \ \phi_1(z) \in \mathcal{P} \text{ and } \mathbf{n}_1(z) = 2k_1 + 2i + 3\}, \ i = 0, \cdots m-1,$$

are non empty disjoint compact subsets of $\mathcal{P}$. Moreover, $(\mathcal{H}_i, \phi_1) : \widehat{\mathcal{P}} \twoheadrightarrow \widehat{\mathcal{Q}}$, for $i = 0, \ldots, m-1$ and assumption (H_{ϕ_1}) of Theorem 1 is satisfied. Similarly, if we denote by $\mathbf{n_2}(z)$ the number of zeros of the y component of the solution of (Eq_2) associated to the initial condition z, then condition a_2) guarantees that

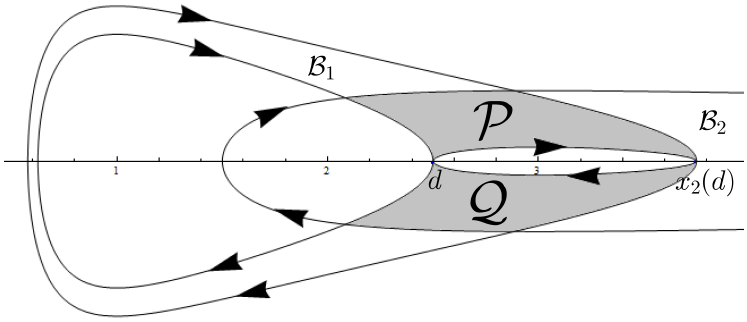

Figure 5.2: Geometry of the linking considered in Theorem 4

the sets

$$\mathcal{K}_j = \{z \in \mathcal{Q} : \ \phi_2(z) \in \mathcal{Q} \text{ and } \mathbf{n}_2(z) = 2k_2 + 2j + 3\}, \ \ j = 0, \cdots l-1,$$

are non empty disjoint compact subsets of $\mathcal{Q}$ and that $(\mathcal{K}_j, \phi_2) : \widehat{\mathcal{Q}} \twoheadrightarrow \widehat{\mathcal{Q}}$, for $j = 0, \ldots, l-1$ and assumption (H_{ϕ_2}) of Theorem 1 is satisfied. We conclude that $\phi = \phi_2 \circ \phi_1$ induces chaotic dynamics on $m \times l$ symbols in

$$\mathcal{H}^* := \bigcup_{\substack{i=0,\ldots,m-1 \\ j=0,\ldots,\ell-1}} \mathcal{H}'_{i,j} \quad \text{with} \ \ \mathcal{H}'_{i,j} := \mathcal{H}_i \cap \phi_1^{-1}(\mathcal{K}_j).$$

The dynamic properties of the chaotic solutions and the stability of the result with respect to small perturbations follow as in Theorem 2. □

In Theorem 4 we consider the remaining case, namely $2h_2 \leq h_1$. In this setting, a first annulus $\mathcal{B}_1$ is constructed with the cycles of (5.1) passing trough $(d, 0)$ and $(x_2(d), 0)$ which are, respectively its inner and outer boundary. A second set $\mathcal{B}_2$ is limited by the cycle of (5.2) through $(d, 0)$ which is its inner boundary and by the parabolic orbit of (5.2) which is its outer boundary (see Figure 5.2). This set is a topological annulus

Theorem 4. *Let us suppose that $h_1 \geq 2h_2$. For a fixed $d \in \left]\frac{\mu^2}{h_1}, \frac{\mu^2}{h_2}\right[$, let us assume that*

$b_1)$ $T_1 > T_1^* = (m+2)\dfrac{T_1(x_2(d))\, T_1(d)}{T_1(x_2(d)) - T_1(d)}$

$b_2)$ $T_2 > lT_2(d)$

Then, system (3.1) *exhibits chaotic dynamics on $m \times l$ symbols. The dynamic properties of the chaotic solutions are as the ones described in Theorem 3 choosing $k_2 = 0$. The result is robust with respect to the small perturbations considered in Theorem 2.*

Remark 1. *The particular links chosen in the above results allow to minimize the lower bound on T which guarantees the existence of chaotic dynamics. In fact, we observe first that the previous conditions can be written in terms of the parameters of the system. More precisely, for values d_1, d_2 which correspond to cycles of (Eq_i), $i = 1, 2$, with d_1 identifying the slower cycle, we have*

$$\Lambda_i(d_1, d_2) = \frac{T_i(d_1)T_i(d_2)}{T_i(d_1) - T_i(d_2)} = \frac{\pi h_i}{\sqrt{2}} \frac{1}{F_i(d_2)^{3/2} - F_i(d_1)^{3/2}}, \quad i = 1, 2. \tag{5.4}$$

Then, fixed μ and h_i, $i = 1, 2$ the continuous function

$$\tau^*(d) = (m+2)\Lambda_1(x_2(d), d) + (l+2)\Lambda_2(\frac{\mu^2}{h_1}, d)$$

$d \in]\frac{\mu^2}{h_1}, \frac{\mu^2}{h_2}[$ provides a lower bound for the period T for which chaotic dynamics occurs in Theorem 3. We can minimize this lower bound by observing that, since

$$\lim_{d \to \frac{\mu^2}{h_1}} \tau^*(d) = \lim_{d \to \frac{\mu^2}{h_2}} \tau^*(d) = +\infty,$$

there exists $d^* \in]\frac{\mu^2}{h_1}, \frac{\mu^2}{2_1}[$ which is a minimum point for τ^* in $]\frac{\mu^2}{h_1}, \frac{\mu^2}{2_1}[$. A similar argument applies to Theorem 4 by minimizing the function

$$\tau^*(d) = (m+2)\Lambda_1(x_2(d), d) + l\frac{\pi h_2}{\sqrt{2}} \frac{1}{[F_2(d)]^{\frac{3}{2}}}$$

in the interval $]\frac{\mu^2}{2h_2}, \frac{\mu^2}{h_2}[$.

6 Chaotic solutions of the Kepler problem with small angular momentum

This last section is devoted to show that, as a consequence of the results of Sections 4 and 5, chaotic solutions may be found in the set of solutions with small angular momentum. As mentioned in the introduction, the rotational symmetry of the system implies that the angular momentum $\mu = |u(t) \wedge \dot{u}(t)|$ is a conserved quantity of the solutions. From now on, we denote by U_μ the set of solutions of system (1.1) with angular momentum μ. Essentially, both the results of this section follows by observing that the inequalities of theorems 2, 3 and 4 may be satisfied for T_1 and T_2 fixed by choosing μ sufficiently small.

In particular, the explicit dependence of $T_1^* \equiv T_1^*(\mu, T_2, m, h_1, h_2)$ on μ in Theorem 2 can be exploited to obtain the following result.

Corollary 1. *Let $h(t)$ be given by (1.3) with $h_1 > 0 > h_2$. Then, for every positive integer $m \geq 2$, there exists μ_m^* such that if $0 < \mu < \mu_m^*$, the set U_μ of solutions of system (1.1) exhibits chaotic dynamics on m symbols. The dynamic properties of the solutions are as in in Theorem 2 and are stable with respect to the small perturbations considered in there.*

Proof. From the proof of Theorem 2 (see (4.4)), we have that

$$T_1^* = mT(\mathcal{C}) = \frac{\pi h_1}{\sqrt{2}}[F_{h_1}(d)]^{-3/2},$$

where $\frac{\mu^2}{2h_1} < d < \frac{\mu^2}{h_1}$ must be chosen sufficiently close to $\frac{\mu^2}{2h_1}$. Then, we take

$$d = \frac{\mu^2}{2h_1}(\mu + 1).$$

Taking this choice, some easy computations give

$$T_1^* = \frac{m\pi}{4h_1^2}(\mu + 1)^3\mu^{3/2}.$$

From here, it is evident that

$$\lim_{\mu \to 0^+} T_1^* = 0,$$

therefore, $T_1^* < T_1$ for μ small enough and Theorem 2 applies. □

Note that Corollary 1 provides chaotic behaviour of solutions with small angular momentum, but we can not provide an explicit bound on how small it should be. However, an explicit quantitative estimate of the smallness of μ can be given in our last result, which deals with the case $h_1 > h_2 > 0$ and which is a direct consequence of theorems 3 and 4.

Corollary 2. *Let $h(t)$ be given by (1.3) with $h_1 > h_2 > 0$. Then, for every positive integers $m, l \geq 2$, there exists an explicitly computable number $\mu^*_{m,l} > 0$ such that if $0 < \mu < \mu^*_{m,l}$, the set U_μ of solutions of system (1.1) exhibits chaotic dynamics on $m \times l$ symbols. The dynamic properties of the solutions are as in Theorem 3 and Theorem 4. This result is stable with respect to the small perturbations considered in Theorem 2.*

Proof. We will focus on the case $h_1 < 2h_2$, since the computations for the remaining case $h_1 \geq 2h_2$ are analogous. Following Remark 1, conditions $a_1)-a_2)$ of Theorem 3 read

$$T_1 > T_1^* = (m+2)\Lambda_1(x_2(d), d), \quad T_2 > T_2^* = (l+2)\Lambda_2\left(\frac{\mu^2}{h_1}, d\right), \tag{6.1}$$

where $d \in]\frac{\mu^2}{h_1}, \frac{\mu^2}{h_2}[$. To find an explicit expression, we may choose the middle point of the interval, $d = \frac{\mu^2}{2h_1h_2}(h_1 + h_2)$. Then, some simple computations give

$$x_2(d) = \frac{h_2}{F_2(d)} - d = \frac{\mu^2}{2h_2^2}(h_1 + h_2).$$

Now, using the formulas (5.4) and (5.3), tedious but elementary computations lead to

$$\Lambda_1(x_2(d), d) = \frac{\pi h_1}{4}\frac{(h_1 + h_2)^3\mu^3}{h_1^{9/2}h_2^{3/2} - h^3(h_1^2 + h_1h_2 - h_2^2)^{3/2}},$$

and

$$\Lambda_2\left(\frac{\mu^2}{h_1}, d\right) = \frac{2\pi h_2(h_1+h_2)^3\mu^3}{(h_1+h_2)^3(2h_1h_2-h_1^2)^{3/2}-8(h_1h_2^3)^{3/2}}.$$

Therefore, (6.1) holds if and only if

$$\mu^3 < H_1 := \frac{4T_1}{(m+2)\pi h_1(h_1+h_2)^3}\left[h_1^{9/2}h_2^{3/2} - h^3(h_1^2+h_1h_2-h_2^2)^{3/2}\right],$$

and

$$\mu^3 < H_2 := \frac{T_2}{(l+2)2\pi h_2(h_1+h_2)^3}\left[(h_1+h_2)^3(2h_1h_2-h_1^2)^{3/2} - 8(h_1h_2^3)^{3/2}\right].$$

Then, we finish by defining $\mu^*_{m,l} = \min\{H_1^{1/3}, H_2^{1/3}\}$. □

References

[1] B. Aulbach and B. Kieninger, On three definitions of chaos, *Nonlinear Dyn. Syst. Theory* **1** (2001), 23–37.

[2] A.A. Bekov, Periodic solutions of the Gylden-Merscherskii problem, Astron. Rep. 37 (1993), 651-654.

[3] K. Burns and H. Weiss, A geometric criterion for positive topological entropy, *Comm. Math. Phys.* **172** (1995), 95–118.

[4] A. Deprit, The secular accelerations in Gylden's problem, Celestial Mechanics, 31 (1983), 1-22.

[5] J. Kennedy e J.A. Yorke, Topological horseshoes, *Trans. Amer. Math. Soc.* **353** (2001), 2513–2530.

[6] J. Chu, P.J. Torres, F. Wang, Radial stability of periodic solutions of the Gylden-Meshcherskii-type problem, *Discrete and Continuous Dynamical Systems A* **35**, Iss.5 (2015) 1921–1932.

[7] A. Medio, M. Pireddu and F. Zanolin, Chaotic dynamics for maps in one and two dimensions: a geometrical method and applications to economics, *International Journal of Bifurcation and Chaos*, **19** (2009) 3283–3309.

[8] A. Margheri, C. Rebelo and F. Zanolin, Chaos in periodically perturbed planar Hamiltonian systems using linked twist maps, *J. Differential Equations* **249** (2010), 3233–3257.

[9] K. Mischaikow e M. Mrozek, Isolating neighborhoods and chaos, *Japan J. Indust. Appl. Math.* **12** (1995), 205–236.

[10] D. Papini and F. Zanolin, On the periodic boundary value problem and chaotic-like dynamics for nonlinear Hill's equations, *Adv. Nonlinear Stud.* **4** (2004), 71–91.

[11] A. Pascoletti, M. Pireddu and F. Zanolin, Multiple periodic solutions and complex dynamics for second order ODEs via linked twist maps. *In:* Proceedings of the 8th Colloquium on the Qualitative Theory of Differential Equations (Szeged, 2007), *Electron. J. Qual. Theory Differ. Equ., Szeged*, **14** (2008), 1–32.

[12] A. Pascoletti and F. Zanolin, Example of a suspension bridge ODE model exhibiting chaotic dynamics: a topological approach, *J. Math. Anal. Appl.* **339** (2008), 1179-1198.

[13] A. Pal, D. Selaru, V. Mioc and C. Cucu-Dumitrescu, The Gyldén-type problem revisited: More refined analytical solutions, Astron. Nachr. 327 (2006), 304-308.

[14] W. C. Saslaw, Motion around a source whose luminosity changes, The Astrophysical Journal 226 (1978), 240-252.

[15] D. Selaru, C. Cucu-Dumitrescu and V. Mioc, On a two-body problem with periodically changing equivalent gravitational parameter, Astron. Nachr. 313 (1993), 257-263.

[16] D. Selaru and V. Mioc, Le probleme de Gyldén du point de vue de la théorie KAM, C. R. Acad. Sci. Paris 325 (1997), Série II b, 487-490.

[17] D. Selaru, V. Mioc and C. Cucu-Dumitrescu, The periodic Gyldén-type problem in Astrophysics, AIP Conf. Proc. 895 (2007), 163-170.

[18] R. Srzednicki, A generalization of the Lefschetz fixed point theorem and detection of chaos, *Proc. Amer. Math. Soc.* **128** (2000), 1231–1239.

[19] P.J. Torres, *Mathematical Models with singularities - A Zoo of Singular Creatures*, Atlantis Briefs in Differential Equations, vol. **1**, Atlantis Press, 2015.

[20] P. Walters, *An Introduction to Ergodic Theory*, Graduate Texts in Mathematics, vol. **79**, Springer-Verlag, New York, 1982.